Talanta 183 (2018) 1–10

Contents lists available at ScienceDirect

Talanta

journal homepage: www.elsevier.com/locate/talanta

Fabrication of a novel enzymatic electrochemical biosensor for determination of tyrosine in some food samples

Kambiz Varmira[a], Ghobad Mohammadi[b], Majid Mahmoudi[a], Reza Khodarahmi[c], Khodabakhsh Rashidi[a], Mehdi Hedayati[d], Hector C. Goicoechea[e], Ali R. Jalalvand[a,*]

[a] Research Center of Oils and Fats (RCOF), Food and Drug Administration (FDA), Kermanshah University of Medical Sciences, Kermanshah, Iran
[b] Department of Pharmaceutics, School of Pharmacy, Kermanshah University of Medical Sciences, Kermanshah, Iran
[c] Medical Biology Research Center, Kermanshah University of Medical Sciences, Kermanshah, Iran
[d] Cellular and Molecular Endocrine Research Center, Research Institute for Endocrine Sciences, Shahid Beheshti University of Medical Sciences, Tehran, Iran
[e] Laboratorio de Desarrollo Analítico y Quimiometría (LADAQ), C_atedra de Química Analítica I, Universidad Nacional del Litoral, Ciudad Universitaria, CC 242 (S3000ZAA), Santa Fe, Argentina

ARTICLE INFO

Keywords:
Tyrosine
Tyrosine hydroxylase
Levodopa
Biosensor
High tyrosine foods

ABSTRACT

In this work, fabrication of a novel and ultrasensitive electrochemical biosensor based on immobilization of tyrosine hydroxylase onto palladium-platinum bimetallic alloy nanoparticles/chitosan-1-ethyl-3-methylimidazolium bis(trifluoromethylsulfonyl) imide/graphene-multiwalled carbon nanotubes-IL/glassy carbon electrode for determination of L-tyrosine in some high tyrosine foods including cheese, egg and yogurt was reported. Immobilization of tyrosine hydroxylase onto the surface of the biosensor was performed by cross-linking tyrosine hydroxylase and chitosan through the addition of glutaraldehyde. Enzymatic biosensors employ the affinity and selectivity of catalytically active proteins towards their target molecules and here, the tyrosine hydroxylase selectively catalyzes the conversion of tyrosine to levodopa which can be oxidized at lower potentials than tyrosine. The modifications were characterized by electrochemical impedance spectroscopy, cyclic voltammetry, energy dispersive X-ray spectroscopic and scanning electron microscopy. Under optimal conditions, the biosensor detected tyrosine in concentration ranges of 0.01×10^{-9} to 8.0×10^{-9} mol L^{-1} and 8.0×10^{-9} to 160.0×10^{-9} mol L^{-1} with a limit of detection of 0.009×10^{-9} mol L^{-1}. The biosensor was able to selective determination of tyrosine even in the presence of common interferents therefore, the biosensor was highly selective. The biosensor also showed good operational stability, antifouling properties, sensitivity, repeatability and reproducibility.

1. Introduction

L-Tyrosine (Tyr) is one of the amino acids which is necessary for the maintenance of nutritional balance. The content of Tyr in the body is correlated to the healthy state of the person [1,2]. Tyr is a precursor for thyroxin, dopa, dopamine, noradrenalin and adrenalin as the hormone or non-tuberculosis mycobacterial in central nervous systems [3]. Tyr can be made in the body of a person who receives enough amounts of phenylalanine. People suffering from Phenylketonuria typically take tyrosine supplements since they cannot consume phenylalanine. Some studies revealed that high Tyr foods such as cheese, lamb, soybeans, pork, fish, beef, chicken, nuts, seeds, eggs, dairy, beans, and whole grains can improve people's memory under stress [1,2]. Some diseases such as hypochondrium, depression and other psychological diseases can be observed in the absence of Tyr [4,5]. Therefore, due to the nutritional importance of Tyr, efficient analytical methods are needed for its determination in food samples. Many analytical methods such as chemiluminescence, fluorometric methods, spectrometric analysis, high performance liquid chromatography and capillary electrophoresis have been reported for the determination of Tyr [6–10]. However, most of these methods are limited by some disadvantages such as cost, time of the analysis and sample preparation. Electrochemical methods provide a simple, low-cost and fast way for analysing biologically and environmentally important substances. Unfortunately, amino acids have a poor electrochemical response at solid electrodes therefore, chemical modifications are employed to improve their electrochemical response. The most important drawback of these chemically modified electrodes is subjected to the rapid surface fouling. This trouble could be tackled by immobilizing an appropriate enzyme at the electrode surface [11]. Enzymatic biosensors are the most widely investigated electrochemical

* Corresponding author.
E-mail address: ali.jalalvand1984@gmail.com (A.R. Jalalvand).

https://doi.org/10.1016/j.talanta.2018.02.053
Received 15 January 2018; Received in revised form 10 February 2018; Accepted 12 February 2018
Available online 13 February 2018
0039-9140/

sensors from applications point of view.

Graphene (Gr) is a monolayer of sp^2 bonded carbons with specific electronic, mechanical and thermal characteristics which is used in different fields of research [12]. Gr has received a lot of applications in electronics, batteries, fuel cells, supercapacitors and biosensors due to its interesting physicochemical properties. On the other hand, carbon nanotubes (CNTs) are rolled graphene sheets which also exhibit good mechanical, electrical and electrocatalytic properties [12]. In recent years, a lot of projects have been focused on applications of CNTs to fabrication of electrochemical sensors and biosensors [13]. Incorporation of Gr with multi-walled carbon nanotubes (MWCNTs) yields a hybrid material with excellent electrocatalytic properties [12]. Ionic liquids (ILs) are another important materials with unique properties such as high ionic conductivity, wide electrochemical window and good thermal stability with a lot of applications sensors and biosensors, in lithium batteries, solar cells and capacitors. Furthermore, carbon nanomaterials-IL composites due to π-π or cation-π interactions have potential applications in fabricating electrochemical sensors and biosensor [14]. Chitosan (Ch) is a natural biopolymer which has excellent properties such as biocompatibility, nontoxicity, film forming ability, good water permeability and high mechanical strength [15–17]. Ch is able to accumulating metallic ions by several mechanisms such as electrostatic attraction, chelation and ion exchange. It has been proven by the other researchers that combination of Ch with ILs can improve properties of Ch [18]. The amine groups of Ch can interact with the nanoparticles (NPs), blocking the aggregation of nanoparticles and as a result dispersed nanoparticles are obtained. Electrodeposition is a controllable method for the synthesis of metallic NPs where density, size, shape and composition of alloy NPs can be controlled by instrumental parameters [19–22]. Alloy NPs have been frequently used in sensing and bio-sensing fields [19–22]. Due to the interaction between components in alloy NPs, they show better properties such as high catalytic activity and selectivity and better resistance to deactivation in comparison with monometallic NPs. Tyrosine hydroxylase (TyrH) catalyzes a reaction in which Tyr is hydroxylated in the meta position to obtain L-3,4-dihydroxyphenylalanine (levodopa, L-DOPA), Scheme 1.

In this work, we are going to fabricate a novel and ultrasensitive Tyr biosensor based on immobilization of TyrH onto palladium-platinum (PdPt) bimetallic alloy nanoparticles (NPs)/chitosan-ionic liquid (Ch-IL)/graphene-multiwalled carbon nanotubes-ionic liquid (Gr-MWCNTs-IL)/glassy carbon electrode (GCE) for determination of Tyr in some high Tyr food samples. Schematic representation of the fabrication steps of the Tyr biosensor is shown in Scheme 2. Immobilization of TyrH onto the surface of the biosensor is performed by cross-linking TyrH and Ch through the addition of glutaraldehyde (GA). After characterization of the modifications by electrochemical and microscopic methods, the biosensor will be analytically characterized and then, will be applied to some high tyrosine foods including cheese, egg and yogurt for determination of Tyr. Finally, the results of the electroanalytical methodology developed in this study will be compared with high performance liquid chromatography (HPLC) with fluorescence detection as reference method to validate its performance.

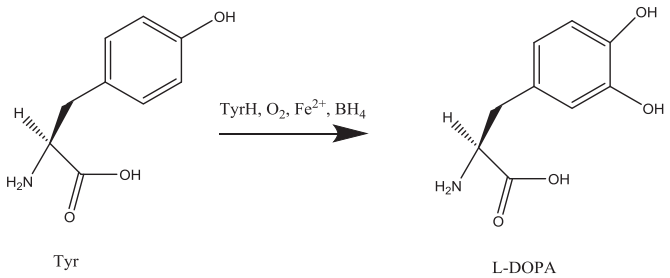

Tyr L-DOPA

Scheme 1. Tyrosine hydroxylase catalyzes conversion of Tyr to L-DOPA.

2. Experimental

2.1. Chemicals and solutions

Tyr, TyrH, Ch, 1-ethyl-3-methylimidazolium bis(trifluoromethylsulfonyl) imide (IL), potassium ferrocyanide, potassium ferriccyanide, palladium (II) chloride ($PdCl_2$), hexachloroplatinic acid (H_2PtCl_6), dimethylformamide (DMF), glutaraldehyde (GA), $NaBH_4$, ferrous chloride tetrahydrate, acetic acid, sodium phosphate monobasic (NaH_2PO_4), sodium phosphate dibasic (Na_2HPO_4), phosphoric acid (H_3PO_4) and sodium hydroxide (NaOH) were purchased from Sigma. Gr was purchased from PubChem. The MWCNTs were prepared from Ionic Liquid Technologies. The other chemicals used in this study were purchased from regular sources and used as received. All the solutions used in this work were prepared in doubly distilled deionized water (DDW).

NaH_2PO_4, and Na_2HPO_4 were used to prepare a phosphate buffered solution (PBS, 0.05 mol L^{-1}) and 1% $NaBH_4$ and 1% ferrous chloride tetrahydrate were added to it and subsequently H_3PO_4 and NaOH were used to adjust its pH at 2.0. The redox probe solution, $[Fe(CN)_6]^{3-/4-}$, with a concentration of 0.05 M was prepared in the 0.1 KCl and used for electrochemical characterization of the modifications. A stock solution of Tyr (0.1 mol L^{-1}) was prepared in the PBS (0.05 mol L^{-1}, pH 2.0) and kept in a refrigerator which was used to prepare Tyr working solutions by applying appropriate dilutions. A stock solution of Ch (0.2%) was prepared in acetic acid (1.0% (v/v)) by ultrasonication for 30.0 min. A mixture of Ch-IL was prepared by adding 1.0 μL IL into 1.0 mL Ch (0.2%). To prepare Gr-MWCNTs-IL, 1.0 mg Gr, 1.0 mg MWCNTs and 5.0 μL IL were added to 3.0 mL DMF and ultrasonicated for 1.0 h. A 0.25% GA solution was prepared by diluting its original solution. A solution containing 2.5×10^{-3} mol L^{-1} H_2PtCl_6, 2.5×10^{-3} mol L^{-1} $PdCl_2$, and 0.1 mol L^{-1} KCl was prepared in the DDW. TyrH was dissolved in the PBS (0.05 mol L^{-1}, pH 2.0) and kept at − 23.0 °C.

2.2. Instruments and softwares

All the electrochemical data obtained from voltammetric and EIS experiments were recorded by an Autolab PGSTAT302N-high performance controlled by the NOVA 2.1.2 software. Chromatographic analyses of real samples were performed by a Shimadzu liquid chromatograph controlled by the Clarity chromatography software which was equipped with LC-10ADvp solvent delivery system, SIL-10ADvp autosampler, CTO-10ASvp column oven, RF-10Axl fluorescence detector and SLC-10Avp system controller. The SEM images were captured by a KYKY-EM 3200 scanning electron microscope. Elemental analyses were performed by an EDS-integrated Hitachi S-4800. A Sigma centrifuge was used to centrifuging the solutions. A JENWAY-3345 pH-meter equipped with a combined glass electrode was applied to pH adjustments. All the recorded electrochemical data was transferred into the MATLAB (Version 7.14, MathWorks, Inc.) environment for baseline corrections by asymmetric least squares splines regression (AsLSSR). Computations based on elliptical joint confidence region (EJCR) were also performed in MATLAB environment. All the computations were performed on a DELL XPS laptop (L502X).

2.3. Fabrication of the biosensor

The GCE was well polished on a silky pad leached by an alumina slurry and then, rinsed with DDW and ultrasonicated in ethanol for 20.0 min and dried at room temperature. 10.0 μL of Gr-MWCNTs-IL solution was dropped onto the surface of the cleaned GCE and left to be dried at room temperature. Then, 5.0 μL of Ch-IL was dropped onto the surface of Gr-MWCNTs-IL/GCE to prepare the Ch-IL/Gr-MWCNTs-IL/GCE and dried under a stream of hot air provided by a hairdryer. For electrochemical synthesis of PdPt bimetallic alloy NPs, the Ch-IL/Gr-MWCNTs-IL/GCE was used as working electrode in an electrochemical

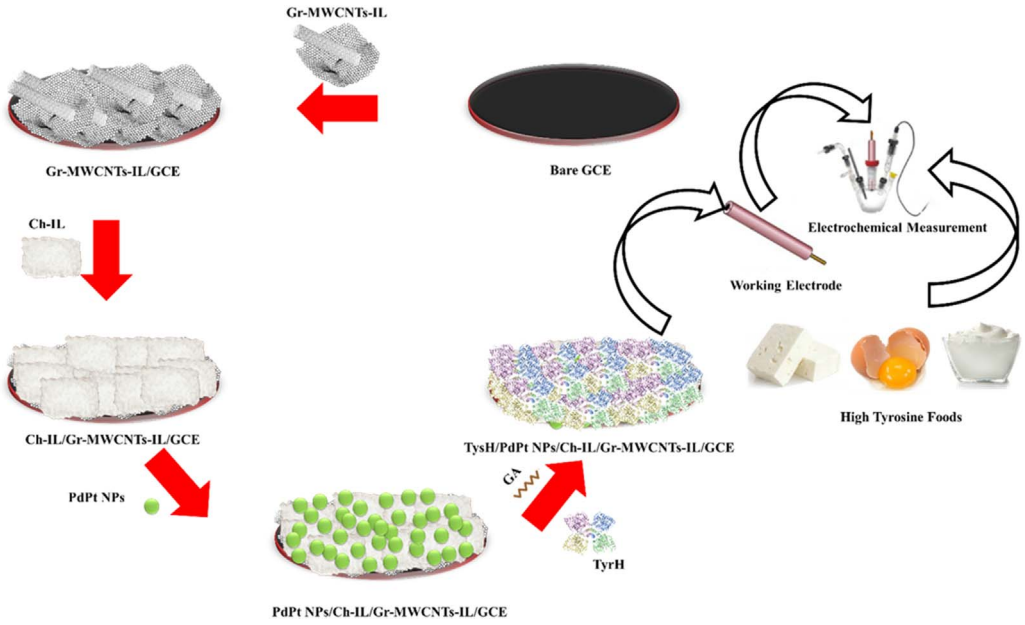

Scheme 2. Schematic representation of the fabrication steps of the Tyr biosensor proposed in this study.

cell containing 10 mL of a solution consisting of 2.5×10^{-3} mol L^{-1} H_2PtCl_6, 2.5×10^{-3} mol L^{-1} $PdCl_2$ and 0.1 mol L^{-1} KCl where Ag/AgCl and Pt wire were acted as reference and counter electrode, respectively. Electrochemical deposition of PdPt bimetallic alloy NPs was performed by cyclic voltammetry (CV) with scanning potential (scan rate = 0.025) from 0 to −0.5 V for 5.0 cycles. Then, the PdPt NPs/Ch-IL/Gr-MWCNTs-IL/GCE was immersed into the 0.25% GA solution for 1.0 h. Finally, 5.0 μL of TyrH solution was dropped onto the surface of the PdPt NPs/Ch-IL/Gr-MWCNTs-IL/GCE and allowed to be dried at room temperature and kept in a refrigerator at −23.0 °C until analysis time.

2.4. Preparation of real samples

Three real samples including yogurt, egg and cheese were purchased from a local supermarket, Kermanshah, Iran. Exact amounts from each sample, egg (50.0 g), yogurt (20.0 g) and cheese (10.0 g) were incubated with hydrochloric acid (2.25 mol L^{-1}, 30.0 mL) at 100.0 °C for 2.0 h and these samples were centrifuged for 15.0 min at 4500.0 rpm and the supernatants were filtered. Then, 10.0 mL of each filtrate was treated with the PBS (0.05 mol L^{-1}, pH 2.0, 10 mL) for further sample assay. Finally, the Tyr concentration was ascertained from the calibration curve by applying an appropriate dilution factor.

3. Results and discussion

3.1. Step-by-step characterizations of the modifications

3.1.1. Electrochemical characterizations

Electrochemical impedance spectroscopy (EIS) is an effective electrochemical method which could be used for monitoring the modifications applied to the bare GCE. The Nyquist plot of the EIS has a semicircle portion at high frequencies which is related to the electron transfer limited process and a linear portion which is corresponded to the diffusion process. The diameter of the semicircle portion is proportional to the resistance of electron transfer (R_{ct}) at the electrode surface which is able to describe the interface properties of the electrode surface. Therefore, according to information described above, we used the EIS method to monitor the modifications applied to the bare GCE. The EIS measurements were performed in an electrochemical cell containing the redox probe solution where a bare or modified GCE acted as working electrode, Pt wire as counter electrode and Ag/AgCl as reference electrode. The R_{ct} values of the EIS curves were calculated by fit and simulation command provided by the NOVA software. The Nyquist plots of the bare GCE (curve a), Gr-MWCNTs-IL/GCE (curve b), Ch-IL/Gr-MWCNTs-IL/GCE (curve c), PdPt NPs/Ch-IL/Gr-MWCNTs-IL/GCE (curve d) and TyrH/PdPt NPs/Ch-IL/Gr-MWCNTs-IL/GCE (curve e) are showing in Fig. 1A. After fitting the EIS curve of the bare GCE, its R_{ct} value was calculated to be 977 Ω. After modifying the bare GCE with Gr-MWCNTs-IL, its R_{ct} value was decreased (38 Ω) which confirmed this layer enhanced the electron transfer rate at the electrode surface. The presence of Ch-IL on the electrode surface increased the R_{ct} value (368 Ω) which manifested that the Ch hindered electron transfer at the electrode surface in some extent. After electrodeposition of PdPt NPs onto the surface of Ch-IL/Gr-MWCNTs-IL/GCE, the R_{ct} value was sharply decreased (14 Ω) which suggested a significant acceleration for redox probe reaction at the electrode surface by opening a lot of new conduction pathways to facilitate electron transfer between electrode surface and electrolyte solution. Finally, immobilization of the TyrH onto the PdPt NPs/Ch-IL/Gr-MWCNTs-IL/GCE surface increased the R_{ct} value (40 Ω) which showed that the TyrH was able to hinder the interfacial electron transfer in some extent.

The CV is also a very useful technique which can help us to monitor the modification steps. Therefore, the CVs of the bare or modified GCEs were recorded in redox probe solution and are showing in Fig. 1B. The bare GCE showed a well-defined CV (curve a) which was really improved (larger peak currents and lower peak potential separation) after modification with Gr-MWCNTs-IL (curve b) manifesting larger electroactive surface area and faster electron transfer for Gr-MWCNTs-IL/GCE. After dropping the Ch-IL onto the Gr-MWCNTs-IL/GCE surface, a poorer CV response with shorter peak currents was recorded (curve c) which confirmed that the Ch hindered the charge transfer at the electrode surface in some extent. By electrodeposition of NPs onto the Ch-IL/Gr-MWCNTs-IL/GCE surface, peak potential separation was decreased while peak currents was increased (curve d) which confirmed the excellent role of NPs in expanding the electroactive surface area and fastening the rate of electron transfer. After immobilization of the TyrH onto the PdPt NPs/Ch-IL/Gr-MWCNTs-IL/GCE surface, the peak currents were decreased and peak separation was increased (curve e) which confirmed that the enzyme molecules were able to block the interface in some extent and decrease the rate of electron transfer.

In order to further characterization of the modification steps, we have

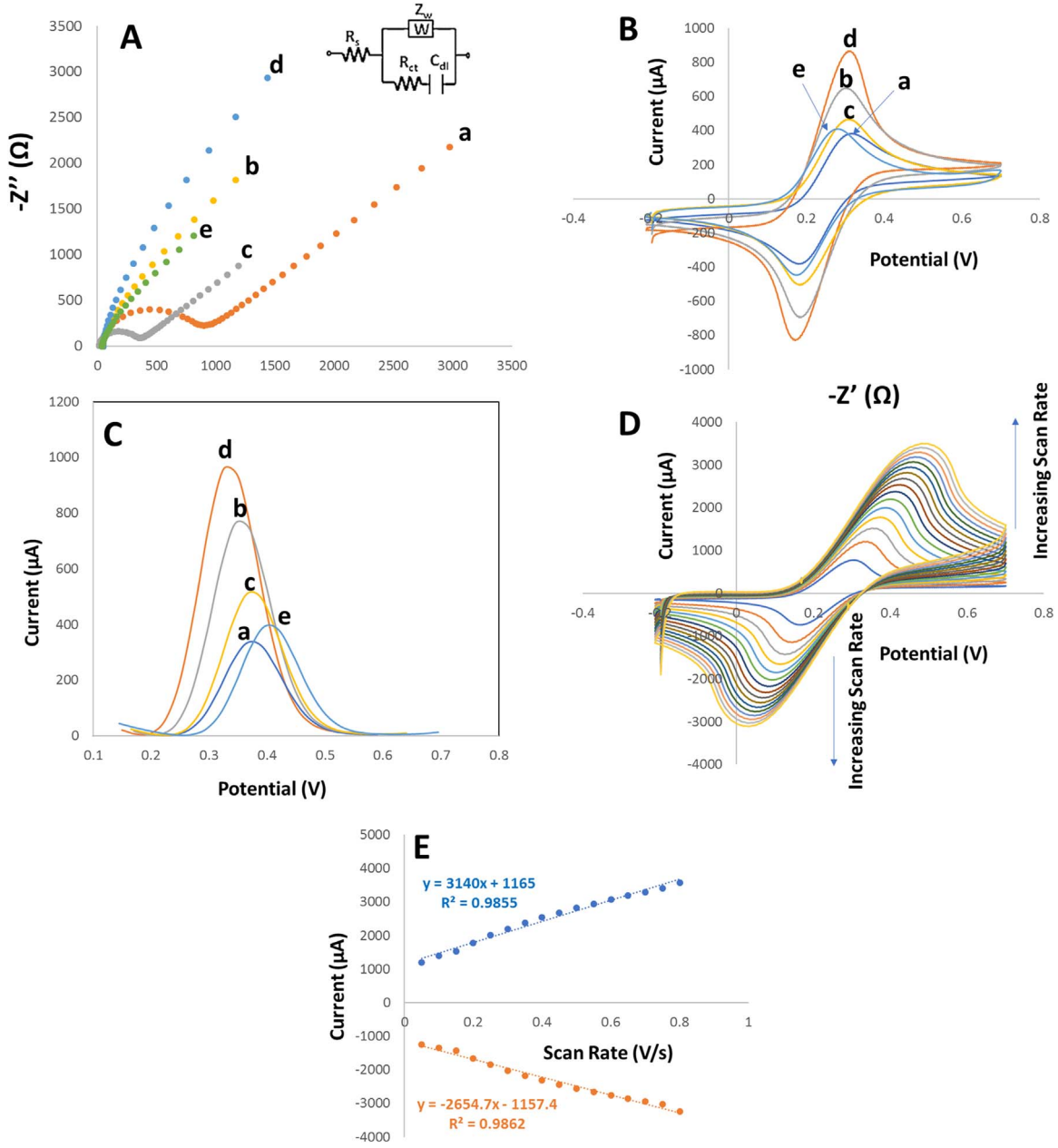

Fig. 1. (A), (B) and (C) EIS spectra, CVs and DPVs of (a) bare GCE, (b) Gr-MWCNTs-IL/GCE, (c) Ch-IL/Gr-MWCNTs-IL/GCE, (d) PdPt NPs/Ch-IL/Gr-MWCNTs-IL/GCE and (e) TyrH/PdPt NPs/Ch-IL/Gr-MWCNTs-IL/GCE in the redox probe solution, respectively. Inset of (A) shows the circuit used to fit the EIS curves where R_s: solution resistance, R_{ct}: electron transfer resistance, C_{dl}: double layer capacitance, Z_w: Warburg impedance, (D) the CVs of TyrH/PdPt NPs/Ch-IL/Gr-MWCNTs-IL/GCE immersed into the redox probe solution at different scan rates (0.05–0.8 V) and (E) variation of peak currents versus scan rates obtained from immersing TyrH/PdPt NPs/Ch-IL/Gr-MWCNTs-IL/GCE into the redox probe solution.

also used differential pulse voltammetry (DPV) experiments in redox probe solution and the results are showing in Fig. 1C. All the DPVs were baseline corrected with the help of AsLSSR and then, they were depicted. As can be seen, after modification of the bare GCE (curve a) with Gr-MWCNTs-IL (curve b), its peak current and peak potential were increased and decreased, respectively. The presence of Ch-IL at the electrode surface as the next layer caused lower peak intensity and higher peak potential as can be clearly observed in curve c. These observation confirmed that the presence of Ch-IL at the electrode surface hinders the electron transfer at the electrode surface in some extent. Electrodeposition of PdPt NPs at the electrode surface caused a more facile electron transfer at the electrode surface (curve d). Immobilization of the TyrH onto the PdPt NPs/Ch-IL/Gr-MWCNTs-IL/GCE surface showed that the enzyme molecules were able to block the interface in some extent and decrease the rate of electron transfer (curve e).

Fig. 1D shows the CVs recorded by TyrH/PdPt NPs/Ch-IL/Gr-MWCNTs-IL/GCE immersed into the redox probe solution at different scan rates (0.05–0.8 V/s). As can be seen, the anodic peaks are shifting toward larger potentials while the cathodic peaks are shifting in the reverse direction by increasing the rate of scanning potentials. The redox peak currents are proportional to the rate of scanning potentials (Fig. 1E) which indicates an adsorption controlled process.

3.1.2. Morphological and structural characterizations

Fig. 2 shows the SEM images captured from the modification steps applied to the bare GCE to fabricate the biosensor. Fig. 2A shows the SEM image of Gr-MWCNTs-IL/GCE which confirms that the Gr sheets and MWCNTs have been attached to the surface of the GCE. Ch-IL formed a layer on the surface of Gr-MWCNTs-IL/GCE as can be observed in Fig. 2B. Fig. 2C shows that the surface of Ch-IL/Gr-MWCNTs-

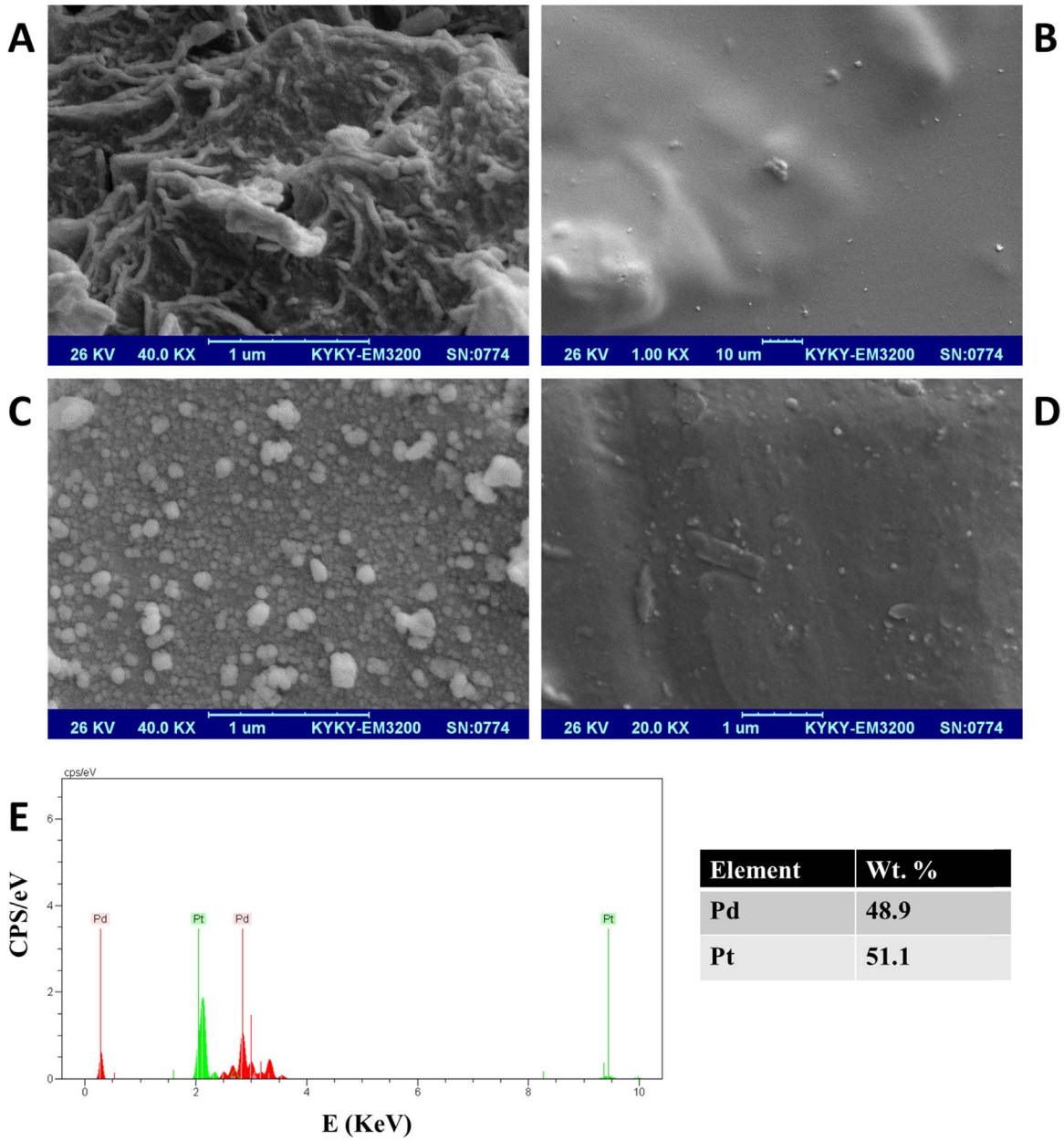

Element	Wt. %
Pd	48.9
Pt	51.1

Fig. 2. The SEM image of (A) Gr-MWCNTs-IL/GCE, (B) Ch-IL/Gr-MWCNTs-IL/GCE, (C) PdPt NPs/Ch-IL/Gr-MWCNTs-IL/GCE and (D) TyrH/PdPt NPs/Ch-IL/Gr-MWCNTs-IL/GCE. (D) Signature peaks obtained by EDS to characterize Pt and Pd.

IL/GCE has been decorated by NPs which also confirms the successfulness of electrochemical deposition of NPs. Finally, Fig. 2D confirms forming a layer onto the surface of PdPt NPs/Ch-IL/Gr-MWCNTs-IL/GCE by the immobilization of TyrH.

Elemental compositions of electrochemically deposited PdPt NPs were characterized by EDS and its results can be observed in Fig. 2E. Signature peaks for Pd and Pt were observed and the weight percentages of Pd and Pt were 48.9% and 51.1%, respectively, which were in good agreement with the molar ratio of metal precursors.

3.2. Performance of different modified electrodes toward Tyr detection

Fig. 3A shows the CVs recorded by bare GCE (curve a), MWCNTs-IL/GCE (curve b), Gr-MWCNTs-IL/GCE (curve c), Ch-IL/Gr-MWCNTs-IL/GCE (curve d), PdPt NPs/Ch-IL/Gr-MWCNTs-IL/GCE (curve e) and TyrH/PdPt NPs/Ch-IL/Gr-MWCNTs-IL/GCE (curve f) as working electrode immersed into a Tyr solution with a concentration level of 100×10^{-6} mol L^{-1} versus Ag/AgCl and Pt wire as reference and counter electrode, respectively. As can be seen, all the modified electrodes have larger peak currents and lower peak potentials in comparison with bare GCE and the best performance has been observed for TyrH/PdPt NPs/Ch-IL/Gr-MWCNTs-IL/GCE which its current is about 205 μA and its potential is 0.83 V. The peak current of TyrH/PdPt NPs/Ch-IL/Gr-MWCNTs-IL/GCE is 7.5 times higher than that of bare GCE (27.1 μA) and its oxidation peak potential (0.83 V) has shifted about 140 mV toward less positive potential in comparison with bare GCE (0.97 V). When oxidation of Tyr at TyrH/PdPt NPs/Ch-IL/Gr-MWCNTs-IL/GCE and PdPt NPs/Ch-IL/Gr-MWCNTs-IL/GCE is compared, there is an obvious enhancement at TyrH/PdPt NPs/Ch-IL/Gr-MWCNTs-IL/GCE which demonstrates that the PdPt NPs/Ch-IL/Gr-MWCNTs-IL can provide a biocompatible microenvironment for TyrH and provides necessary pathways for its direct electron transfer. Fig. 3B shows the responses of bare GCE (curve a), MWCNTs-IL/GCE (curve b), Gr-MWCNTs-IL/GCE (curve c), Ch-IL/Gr-MWCNTs-IL/GCE (curve d), PdPt

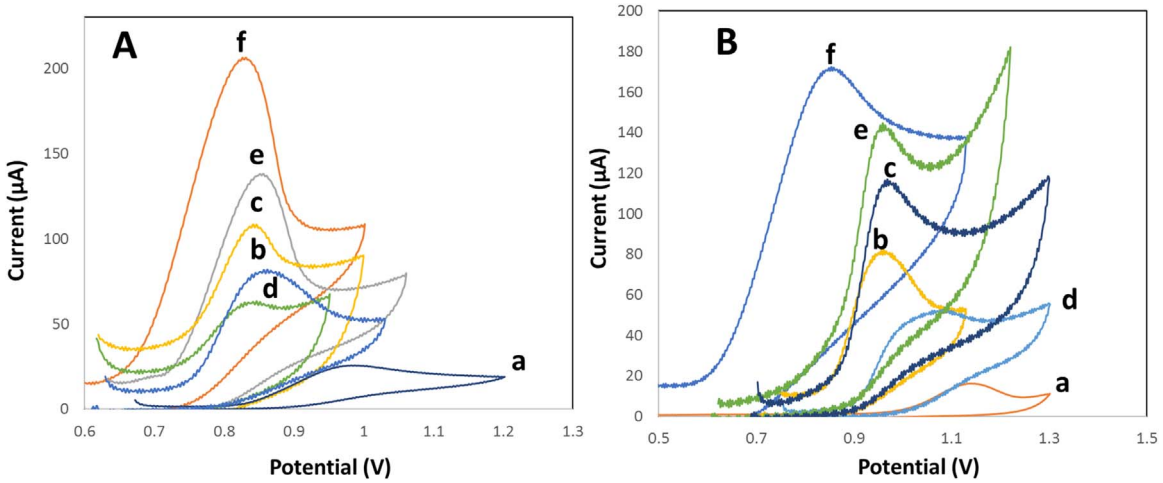

Fig. 3. (A) CVs recorded by (a) bare GCE, (b) MWCNTs-IL/GCE, (c) Gr-MWCNTs-IL/GCE, (d) Ch-IL/Gr-MWCNTs-IL/GCE, (e) PdPt NPs/Ch-IL/Gr-MWCNTs-IL/GCE and (f) TyrH/PdPt NPs/Ch-IL/Gr-MWCNTs-IL/GCE as working electrode immersed into a Tyr solution with a concentration level of 100×10^{-6} mol L^{-1} prepared in the PBS (0.05 mol L^{-1}, pH 2) versus Ag/AgCl and Pt wire as reference and counter electrodes, respectively, scan rate 0.05 V/s and (B) as (A) but in the presence of 100×10^{-6} mol L^{-1} L-DOPA.

NPs/Ch-IL/Gr-MWCNTs-IL/GCE (curve e) and TyrH/PdPt NPs/Ch-IL/Gr-MWCNTs-IL/GCE (curve f) in the presence of L-DOPA. By comparing Fig. 3A and B it can be clearly observed that the oxidation of L-DOPA is occurred at higher potentials than Tyr. TyrH/PdPt NPs/Ch-IL/Gr-MWCNTs-IL/GCE had different responses to L-DOPA and Tyr which may be related to the selective enzymatic response of TyrH to Tyr. Therefore, as a result, it can be concluded that the biosensor has a selective response to Tyr which confirms that the presence of the enzyme at the electrode surface can help to the selectivity of the biosensor.

3.3. Investigation of the pH effects

Oxidation of Tyr is affected by the pH of the solution as it exhibits diverse protonated forms in different pH [23]. By taking into account that for electroanalytical purposes both maximal and stable currents are necessary, we have studied the pH effects on the response of the biosensor. The CVs of TyrH/PdPt NPs/Ch-IL/Gr-MWCNTs-IL/GCE immersed into the PBSs (0.05 mol L^{-1}) with different pHs ranging from 2.0 to 12.0 were recorded and are showing in Fig. 4A. As can be seen in Fig. 4A, the CVs were shifted to less positive potentials with increasing pH and the results show that the maximum current is observed at pH 2 (Fig. 4B) therefore, pH 2 was selected as optimal pH for next studies. As can be seen, the peak potentials are negatively shifted with increasing pH of the PBS with a slope of -0.0558 V pH^{-1} (Fig. 4C) which suggests that the electrode obeys the Nernst behaviour which involves proton and electron in 1:1 ratio (see Scheme 3). This mechanism is in accordance with the mechanism of Tyr oxidation reported elsewhere [24].

3.4. Investigation of the scan rate effects

The CVs of TyrH/PdPt NPs/Ch-IL/Gr-MWCNTs-IL/GCE immersed into a Tyr solution prepared in the PBS (0.05 mol L^{-1}, pH 2) at different scan rates ranging from 0.05 to 0.75 V/s were recorded (Fig. 5A) to investigate the dependence of the currents on the rate of scanning potentials. Regression of peak current values on scan rate values yielded a linear dependence which confirmed that the oxidation of Tyr on the surface of the biosensor is controlled by adsorption (Fig. 5B).

3.5. Analytical characterizations

Since DPV has a much higher sensitivity than CV, it was chosen as the analytical technique for determination of Tyr. Under optimized conditions: step potential 0.025 V, modulation amplitude 0.025 V, modulation time 0.05 s, interval time 0.5 s and scan rate 0.05 V/s, the relationship between DPV responses and concentrations of synthetic Tyr samples was investigated (Fig. 6). The peak current values (I_P) were regressed on the concentration values of Tyr samples (C_{Tyr}) and the results confirmed that there were two linear relationships between I_P and C_{Tyr} over two concentration ranges from 0.01×10^{-9} to 8.0×10^{-9} mol L^{-1} and 8.0×10^{-9} to 160.0×10^{-9} mol L^{-1} as can be seen in the inset of Fig. 6. The linearities observed in the biosensor response over concentration changes show that the biosensor could be possibly applied to the analysis of real samples towards Tyr determination. The limit of detection (LOD) of the developed biosensor was calculated according to IUPAC recommendations ($3S_b$/b, where S_b is

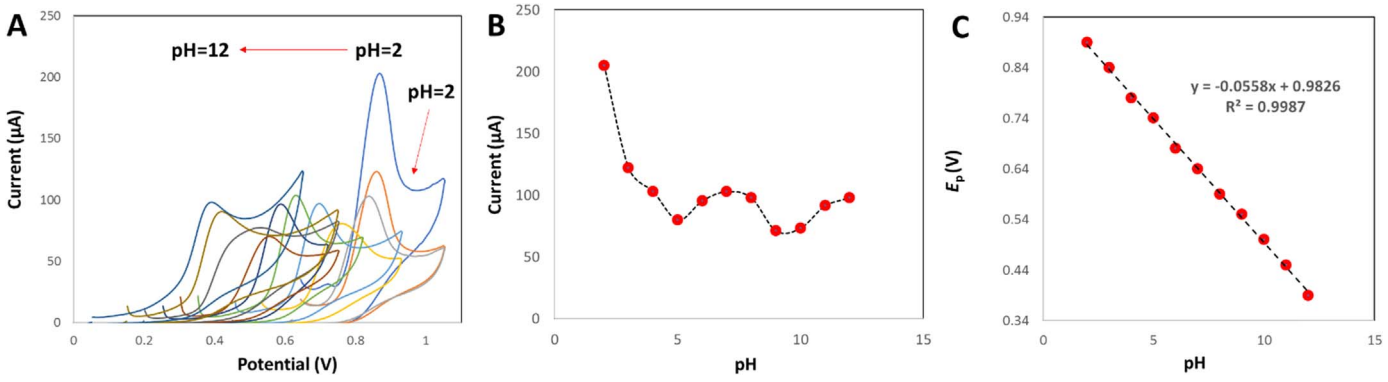

Fig. 4. (A) CVs of TyrH/PdPt NPs/Ch-IL/Gr-MWCNTs-IL/GCE immersed into a Tyr solution (100×10^{-6} mol L^{-1}) prepared in the PBS (0.05 mol L^{-1}) at different pHs, scan rate 0.05 V/s, (B) variation of the peak currents of CVs recorded at different pHs versus pH and (C) variation of peak potentials versus pH.

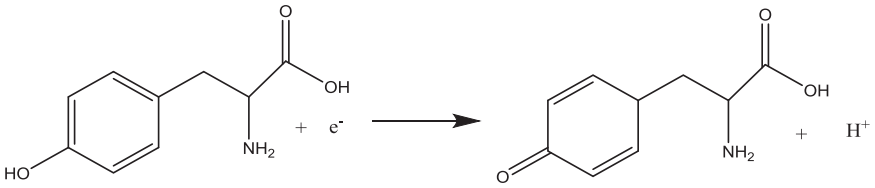

Scheme 3. The proposed mechanism for electro-oxidation mechanism of Tyr.

the standard deviation (n = 8) of the blanks, and *b* is the slope of the calibration curve) at a concentration level of 0.009×10^{-9} mol L^{-1} and the sensitivity of the developed biosensor was calculated to be 0.086 μA $(10^{-9}$ mol $L^{-1})^{-1}$ which confirms a high sensitivity towards Tyr determination. The response time of the biosensor was also calculated to be less than 5 s.

3.6. Comparison with previous works reported in literature

The results obtained by the fabricated biosensor in this study were compared with those of reported by the previous works published in the literature and the results are presented in Table 1. As can be seen, the proposed biosensor showed better results over the most of the reported sensors so far.

3.7. Interference study

To evaluate the selectivity of the constructed Tyr biosensor, the influence of several interfering agents such as urea, sucrose, galactose, boric acid, oxalic acid, L-lysine, L-asparagines, glycine, phenylalanine, N-acetyl-L-cysteine, glutathione, L-cysteine, ascorbic acid, Mg^{2+}, Ca^{2+}, Na^{+}, K^{+} and lactase on the determination of 50×10^{-6} mol L^{-1} Tyr under the optimal experimental conditions was investigated. The tolerance limit was computed as the maximum concentration of the interfering agent which caused an approximately ± 5% relative error in the determination of Tyr concentration. Recording the DPV responses of TyrH/PdPt NPs/Ch-IL/Gr-MWCNTs-IL/GCE towards Try determination in the presence of the interfering agents confirmed that the abided concentration of interfering agents was 0.1 mol L^{-1} for Mg^{2+}, Ca^{2+}, Na^{+} and K^{+}; 0.01 mol L^{-1} for L-lysine, L-asparagines, glycine, phenylalanine, N-acetyl-L-cysteine, ascorbic acid and L-cysteine and 0.001 mol L^{-1} for urea, sucrose, lactase, galactose, boric acid, oxalic acid and glutathione. The results are shown in Table 2. As can be seen, the results confirmed that the TyrH/PdPt NPs/Ch-IL/Gr-MWCNTs-IL/GCE can be considered as a selective electrochemical biosensor for

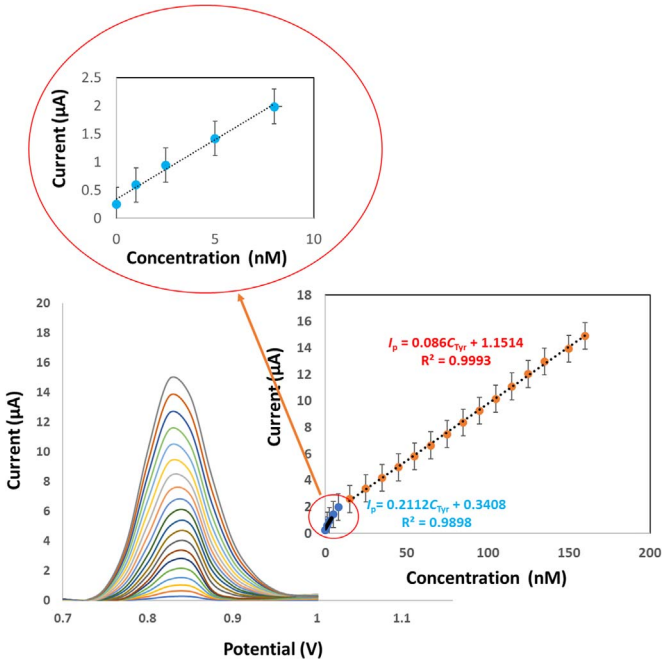

Fig. 6. DPV responses obtained at TyrH/PdPt NPs/Ch-IL/Gr-MWCNTs-IL/GCE upon successive addition of Tyr into PBS (0.05 mol L^{-1}, pH 2). Inset: regression of peak current values on Tyr concentrations with two linear ranges of $0.01 \times 10^{-9} - 8.0 \times 10^{-9}$ mol L^{-1} and $8.0 \times 10^{-9} - 160.0 \times 10^{-9}$ mol L^{-1}.

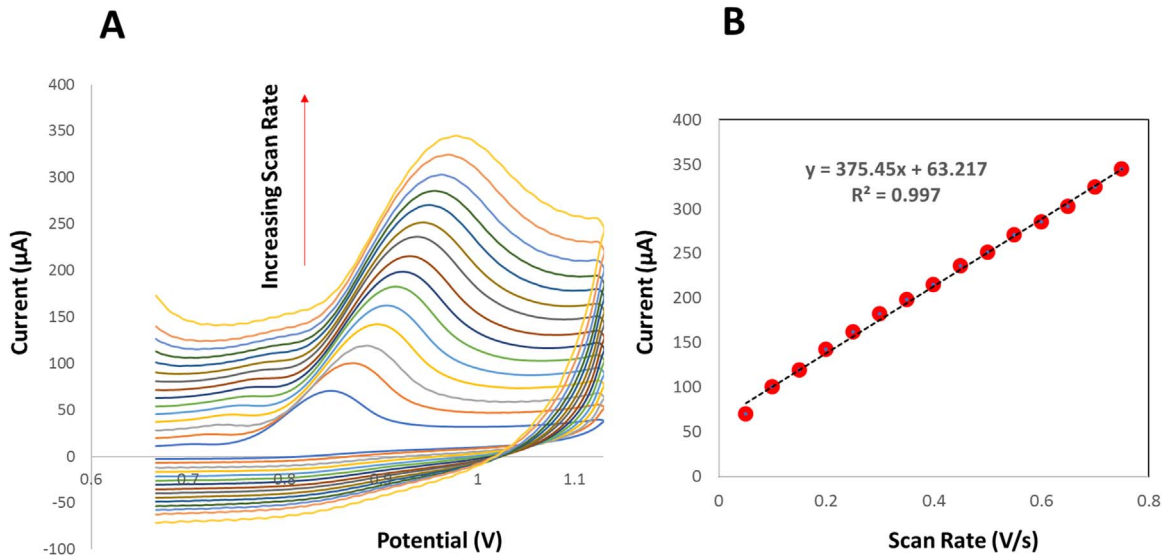

Fig. 5. (A) CVs of TyrH/PdPt NPs/Ch-IL/Gr-MWCNTs-IL/GCE immersed into a Tyr solution (25×10^{-6} mol L^{-1}) prepared in the PBS (0.05 mol L^{-1}, pH 2) at different scan rates ranging 0.05–0.75 V/s and (B) variation of peak current versus scan rate.

Table 1
Comparison of the proposed biosensor with other reported methods for Tyr determination.

Electrode	Linear Rang (mol L^{-1})	LOD (mol L^{-1})	Ref.
MWCNT/4-amino benzene sulfonic acid/GCE	1×10^{-7} to 5×10^{-5}	8×10^{-8}	[25]
MWCNT, GCE	9×10^{-7} to 3.5×10^{-4}	3.5×10^{-7}	[26]
MWCNT, ionic liquid, copper (II)/GCE	1×10^{-8} to 5×10^{-6}	8×10^{-9}	[27]
Polypyrrole, Ni electrode MIP[a]	5×10^{-3} to 4.5×10^{-2}	–	[28]
Cu(II), HMDE[b]	1×10^{-7} to 5×10^{-5}	5×10^{-8}	[29]
Zeolite/carbon paste	1.26×10^{-6} to 9×10^{-5}	3.2×10^{-7}	[30]
Boron-doped diamond electrode	2×10^{-5} to 1×10^{-3}	1×10^{-6}	[31]
MWCNT/GCE	2×10^{-6} to 5×10^{-4}	4×10^{-7}	[32]
Gold nanoparticles/GCE	1×10^{-7} to 3×10^{-4}	4×10^{-8}	[33]
Copper (II), MICP, MIP	1×10^{-8} to 1×10^{-6}	4×10^{-9}	[34]
Fe-hydroxyapatite/tyrosinase	1.0×10^{-7} to 1.1×10^{-5}	2.45×10^{-7} [35]	
β-CD[c] modified gold electrode	3.6×10^{-5} to 2.4×10^{-4}	1.2×10^{-5} [36]	
EuHCF[d] modified graphite electrode	10×10^{-6} to 6×10^{-4}	8.0×10^{-6} [37]	
GCE/SWCNT	5.0×10^{-6} to 2.0×10^{-5}, 2.7×10^{-5} to 2.6×10^{-4}	9.0×10^{-8} [38]	
Au NPs/poly (trisamine)/GCE	3.9×10^{-6} to 61.8×10^{-6}	0.9×10^{-6} [39]	
fMWCNT-Au-HP β-CD/GCE	2.2×10^{-4} to 8.7×10^{-4}	3.0×10^{-4} [40]	
TyrH/PdPt NPs/Ch-IL/Gr-MWCNTs-IL/GCE	0.01×10^{-9} – 8×10^{-9} and 8×10^{-9} – 160×10^{-9}	0.009×10^{-9}	This work

[a] Molecularly imprinted polymer.
[b] Hanging mercury drop electrode.
[c] Cyclodextrin.
[d] Europium hexacyanoferrate film.

Table 2
Effect of potential interfering species on the determination of Tyr at level of 50×10^{-6} mol L^{-1}.

Interfering species	Concentration of interfering species (mol L^{-1})	Found Tyr (mol L^{-1})	Relative error in determination of Tyr (%)	Recovery of Tyr (%)
Mg^{2+}	0.1	5.15×10^{-5}	+3.00	102.91
Ca^{2+}	0.1	5.20×10^{-5}	+4.00	103.84
N^{a+}	0.1	5.10×10^{-5}	+2.00	101.96
K^{+}	0.1	4.95×10^{-5}	−1.00	99.00
L-lysine	0.01	4.80×10^{-5}	−4.00	96.00
L-asparagines	0.01	4.92×10^{-5}	−1.60	98.40
Ascorbic acid	0.01	4.87×10^{-5}	−2.60	97.40
Glycine	0.01	5.06×10^{-5}	+1.20	101.18
Phenylalanine	0.01	5.20×10^{-5}	+4.00	102.34
N-acetyl-L-cysteine	0.01	5.12×10^{-5}	+2.40	98.00
L-cysteine	0.01	4.90×10^{-5}	−2.00	100.00
Urea	0.001	5.00×10^{-5}	0.00	97.80
Sucrose	0.001	4.89×10^{-5}	−2.20	98.00
Lactase	0.001	4.90×10^{-5}	−2.00	102.00
Galactose	0.001	4.78×10^{-5}	−4.40	95.60
Boric acid	0.001	5.13×10^{-5}	+2.60	102.60
Oxalic acid	0.001	5.25×10^{-5}	+5.00	105.00
Glutathione	0.001	5.20×10^{-5}	+4.00	104.00

determination of Tyr.

3.8. Stability, repeatability and reproducibility of the biosensor

Stability is a very important characteristic of a biosensor therefore, to verify the stability of the TyrH/PdPt NPs/Ch-IL/Gr-MWCNTs-IL/GCE, DPV responses of the biosensor towards Tyr determination in a solution containing 10×10^{-9} mol L^{-1} Tyr were weekly recorded during six weeks and the results are shown in Fig. 7. After six weeks, the proposed biosensor retained 94.1% of its initial response. Further verifications towards examining the stability of the biosensor showed that its stability is also affected by the time of immersing into the solution therefore, this parameter was also examined and the results showed that the stability of the biosensor is highly affected by a long time of immersing into the solution and the biosensor doesn't show a good stability by immersing into the cell solution for more than 3.0 h. Therefore, our recommendation to tackle this challenge is to remove

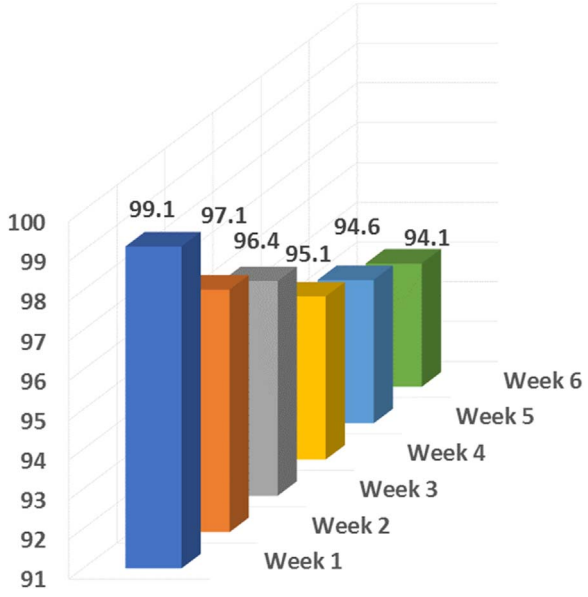

Fig. 7. Stability of DPV responses of the TyrH/PdPt NPs/Ch-IL/Gr-MWCNTs-IL/GCE to Tyr in a solution containing 10×10^{-9} mol L^{-1} Tyr during six weeks.

the biosensor from cell solution during the breaks between the experiments. Repeatability of the proposed biosensor was also investigated by applying it for ten times during a day to determine Tyr in a solution containing 10×10^{-9} mol L^{-1} Tyr and a satisfied relative standard deviation (RSD) of 2.05% was found which confirmed a good repeatability for the biosensor. The reproducibility of the biosensor was also examined by recording the DPV responses of ten individual biosensors immersed into a solution containing 10×10^{-9} mol L^{-1} Tyr and a good RSD value of 2.5% was obtained which confirmed a good reproducibility for the biosensor. The information mentioned above, confirmed that the biosensor response towards Tyr determination was stable, repeatable, and reproducible.

3.9. Application of the fabricated biosensor to real samples and validation of it

Generally, after developing a new analytical method and validating

Table 3
Determination of Tyr in real samples using the proposed biosensor and HPLC as reference method.

Sample	Method	Detected (mol L^{-1})	Added (mol L^{-1})	Found (mol L^{-1})	Recovery (%)
Yogurt	Biosensor	3.41×10^{-6}	1.0×10^{-7}	3.44×10^{-6}	98.01
Yogurt	HPLC	3.63×10^{-6}	1.0×10^{-7}	3.73×10^{-6}	100
Egg	Biosensor	2.21×10^{-7}	1.0×10^{-8}	2.35×10^{-7}	101.7
Egg	HPLC	2.28×10^{-7}	1.0×10^{-8}	2.35×10^{-7}	98.74
Cheese	Biosensor	0.21×10^{-6}	1.0×10^{-7}	0.33×10^{-6}	106.06
Cheese	HPLC	$0.2\ 0\times10^{-6}$	1.0×10^{-7}	$0.32\ \times10^{-6}$	103.1

its performance for the analysis of synthetic samples, its performance is compared with a reference method to verify its capability for the analysis of real samples. Then, the newly developed analytical method could be suggested as a reliable method for routine analyses. Regarding this important step, we have also applied HPLC analysis of the yogurt, cheese and egg as real samples towards Tyr determination and its results are presented in Table 3. As can be seen, good recoveries confirm that there was an acceptable agreement between its results and those obtained by the biosensor fabricated in this study. For making a graphically comparison between accuracy and precision of the HPLC and the proposed biosensor, we have used the EJCR test [41,42]. In this step, yogurt sample as one of real samples was chosen and spiked with 10×10^{-9}, 2×10^{-9}, 100×10^{-9}, 5×10^{-9}, 34×10^{-9}, 68×10^{-9} and 44×10^{-9} mol L^{-1} Tyr and analysed by HPLC and the biosensor. Subsequently, regression of the predicted concentrations by the proposed biosensor and/or HPLC on the nominal concentrations (spiked concentrations) was performed by ordinary least squares, Fig. 8A and B. Then, we used the EJCR test to compare the calculated intercept and slope values with their expected theoretical values (intercept = 0, slope = 1) which is also called "ideal point". Therefore, if the ellipses obtained as the outputs of the EJCR include the ideal point, the predicted and nominal concentrations are not significantly different. The size of ellipses is proportional to the precision of the method, smaller sizes confirm higher precisions [41,42]. Results of the EJCR test are showing in Fig. 8C. As cab be seen, ellipses of both methods contain the ideal point which confirm that both of them are accurate but, the ellipse of HPLC is smaller than that of the proposed biosensor which confirms that the reference method has better precision than the proposed biosensor. According to the results obtained above, the precision of the HPLC was better than the proposed biosensor but, HPLC suffers from some problems such as cost, time and needing a skilled operator and these disadvantages forced us to make a decision for preferring the proposed biosensor.

4. Conclusions

Tyr is one of the amino acids which is necessary for maintenance of nutritional balance and its level in the body is correlated to the healthy state of the person therefore, in this work, enzymatic biosensing of Tyr in some high tyrosine foods including cheese, egg and yogurt was reported according to fabrication of a novel and ultrasensitive electrochemical biosensor based on immobilization of TyrH onto PdPt NPs/Ch-IL/Gr-MWCNTs-IL/GCE. Electro-oxidation of Tyr at TyrH/PdPt NPs/Ch-IL/Gr-MWCNTs-IL/GCE was obviously enhanced which demonstrated that the PdPt NPs/Ch-IL/Gr-MWCNTs-IL provided a biocompatible microenvironment for TyrH and necessary pathways for direct electron transfer. The biosensor could be easily fabricated which showed high sensitivity, selectivity, fast response time and good reproducibility and repeatability towards Tyr determination in both synthetic and real samples. Validation of the developed method by comparing its results with those obtained by HPLC with florescence detection confirmed that the method is reliable and accurate. The biosensor fabricated in this study could be applied for a wide range of

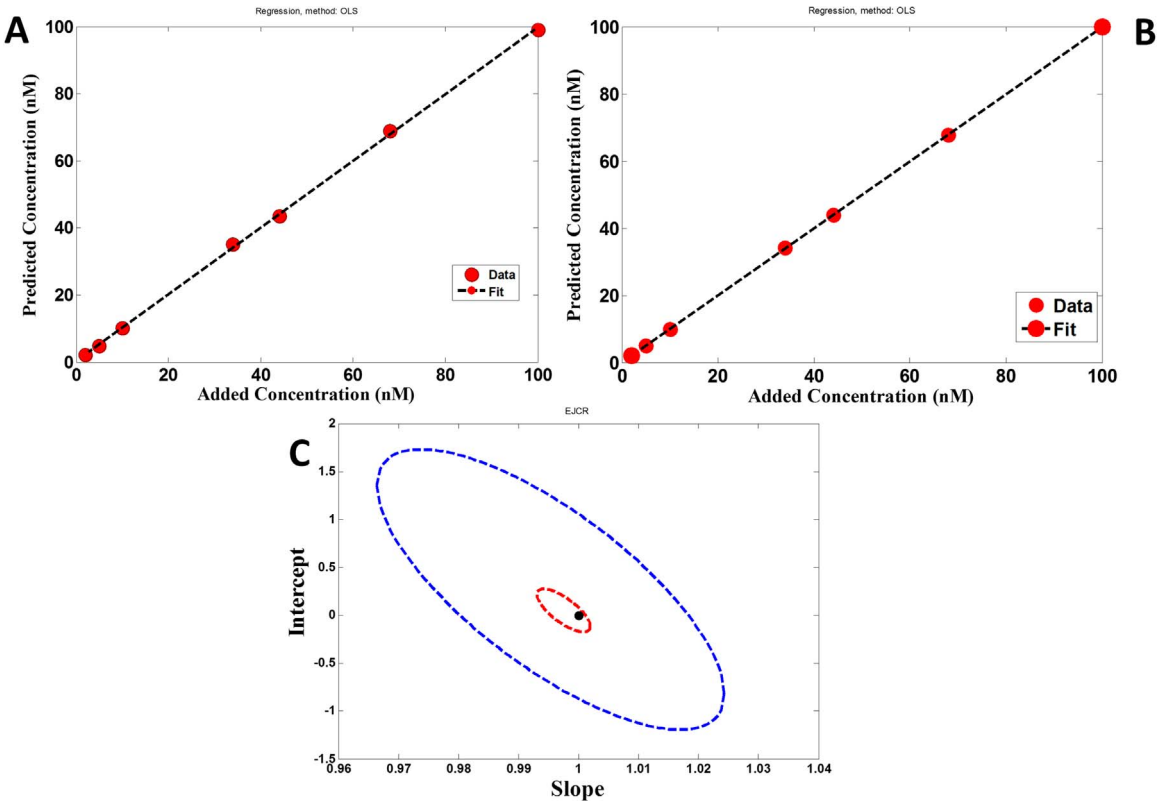

Fig. 8. (A) Plots for regression of predicted concentrations on nominal ones by (A) the proposed biosensor and (B) HPLC. (C) Elliptical joint regions (at 95% confidence level) related to the predictions by the proposed biosensor (blue ellipse) and HPLC (red ellipse), the dark point refers to the ideal point. (For interpretation of the references to color in this figure legend, the reader is referred to the web version of this article.)

applications in routine analyses of Tyr.

Acknowledgements

Financial supports of this project by the research council of Kermanshah University of Medical Sciences are gratefully acknowledged.

Compliance with ethics requirements

This work does not have any studies with humans or animals.

Conflict of interests

Here, we declare that we have no conflict of interest.

References

[1] A. Carlsson, M. Lindqvist, N.S. Arch, Dependence of 5-HT and catecholamine synthesis on concentrations of precursor amino-acids in rat brain, Pharmacology 303 (1978) 157–164.
[2] J.P. Jin, X.Q. Lin, The electrochemical behavior and amperometric determination of tyrosine and tryptophan at a glassy carbon electrode modified with butyrylcholine, Electrochem. Commun. 6 (2004) 454–460.
[3] G. Beck, C. Hanusch, P. Brinkkoetter, N. Rafat, J. Schulte, K. Ackern, B. Yard, Effekte von Dopamin auf die zelluläre und humorale Immunantwort von Patienten mit Sepsis, Anaesthesist 54 (2005) 1012–1020.
[4] O.Y. Al-Dirbashi, M. Jacob, L.Y. Al-Ahaidib, K. Al-Qahoni, Z. Rahbeeni, M. Al-Owain, M.S. Rashed, Quantification of succinylacetone in urine of hepatorenal tyrosinemia patients by HPLC with fluorescence detection, Clin. Chim. Acta 365 (2006) 243–248.
[5] C.Y. Li, Voltammetric determination of tyrosine based on an L-serine polymer film electrode, Colloids Surf. B 50 (2006) 147–151.
[6] F. Wang, K.Z. Wu, Y. Qing, Y.X. Ci, Spectrofluorimetric determination of the substrates based on the fluorescence formation with the peroxidase-like conjugates of hemie, Anal. Lett. 25 (1992) 1469–1478.
[7] S. Alonso, L. Zamora, M. Calatayud, Determination of tyrosine through a FIA-direct chemiluminescence procedure, Talanta 60 (2003) 369–376.
[8] C.J. Lee, J. Yang, α-cyclodextrin-modified infrared chemical sensor for selective determination of tyrosine in biological fluids, Anal. Biochem. 359 (2006) 124–131.
[9] Y. Ishii, M. Iijima, T. Umemura, A. Nishikawa, Y. Iwasaki, R. Ito, K. Saito, M. Hirose, H. Nakazawa, Determination of nitrotyrosine and tyrosine by high-performance liquid chromatography with tandem mass spectrometry and immunohistochemical analysis in livers of mice administered acetaminophen, J. Pharm. Biomed. Anal. 41 (2006) 1325–1331.
[10] Y. Huang, X.Y. Jiang, W. Wang, J.P. Duan, G. Chen, Separation and determination of L-tyrosine and its metabolites by capillary zone electrophoresis with a wall-jet amperometric detection, Talanta 70 (2006) 1157–1163.
[11] H.B. Yildiz, R. Freeman, R. Gill, I. Willner, Electrochemical, photoelectrochemical, and piezoelectric analysis of tyrosinase activity by functionalized nanoparticles, Anal. Chem. 80 (2008) 2811–2816.
[12] V. Mani, B. Devadas, S.-M. Chen, Direct electrochemistry of glucose oxidase at electrochemically reduced graphene oxide-multiwalled carbon nanotubes hybrid material modified electrode for glucose biosensor, Biosens. Bioelectron. 15 (2013) 309–315.
[13] C.B. Jacobs, M.J. Peairs, B.J. Venton, Review: carbon nanotube based electrochemical sensors for biomolecules, Anal. Chim. Acta 662 (2010) 105–127.
[14] W. Zhu, Y. Zhou, J. Zhang, Direct electrochemistry and electrocatalysis of myoglobin based on silica-coated gold nanorods/room temperature ionic liquid/silica sol-gel composite film, Talanta 80 (2009) 224–230.
[15] M. Zhang, A. Smith, W. Gorski, Carbon nanotube-chitosan system for electrochemical sensing based on dehydrogenase enzymes, Anal. Chem. 76 (2004) 5045–5050.
[16] J. Lin, W. Qu, S. Zhang, Disposable biosensor based on enzyme immobilized on Au–chitosan-modified indium tin oxide electrode with flow injection amperometric analysis, Anal. Biochem. 360 (2007) 288–293.
[17] K. Varmira, O. Abdi, M.-B. Gholivand, H.C. Goicoechea, A.R. Jalalvand, Intellectual modifying a bare glassy carbon electrode to fabricate a novel and ultrasensitive electrochemical biosensor: application to determination of acrylamide in food samples, Talanta 176 (2018) 509–517.
[18] F. Xiao, F. Zhao, Y. Zhang, G. Guo, B. Zeng, Ultrasonic electrodeposition of gold-platinum alloy nanoparticles on ionic liquid-chitosan composite film and their application in fabricating nonenzyme hydrogen peroxide sensors, J. Phys. Chem. C 113 (2009) 849–855.
[19] J.C. Claussen, A.D. Franklin, A. ul Haque, D.M. Porterfield, T.S. Fisher, Electrochemical biosensor of nanocube-augmented carbon nanotube networks, ACS Nano 3 (2009) 37–44.
[20] J. Yang, W.-D. Zhang, S. Gunasekaran, An amperometric non-enzymatic glucose sensor by electrodepositing copper nanocubes onto vertically well-aligned multi-walled carbon nanotube arrays, Biosens. Bioelectron. 26 (2010) 279–284.
[21] M.-B. Gholivand, A.R. Jalalvand, H.C. Goicoechea, G. Paimard, T. Skov, Surface exploration of a room-temperature ionic liquid-chitin composite film decorated with electrochemically deposited PdFeNi trimetallic alloy nanoparticles by pattern recognition: an elegant approach to developing a novel biotin biosensor, Talanta 131 (2015) 249–258.
[22] M.-B. Gholivand, A.R. Jalalvand, H.C. Goicoechea, Computer-assisted electrochemical fabrication of a highly selective and sensitive amperometric nitrite sensor based on surface decoration of electrochemically reduced graphene oxide nanosheets with CoNi bimetallic alloy nanoparticles, Mater. Sci. Eng. C 40 (2014) 109–120.
[23] C.J. Lee, J. Yang, α-cyclodextrin-modified infrared chemical sensor for the selective determination of tyrosine in biological fluids, Anal. Biochem. 359 (2006) 124–131.
[24] Q. Xu, S.F. Wang, Electrocatalytic oxidation and direct determination of L-tyrosine by square wave voltammetry at multi-wall carbon nanotubes modified glassy carbon electrodes, Microchim. Acta 151 (2005) 47–52.
[25] K. Huang, D. Luo, W. Xie, Y. Yu, Sensitive voltammetric determination of tyrosine using multi-walled carbon nanotubes/4-aminobenzeresulfonic acid film-coated glassy carbon electrode, Colloids Surf. B 61 (2008) 176–181.
[26] J. Xu, Y. Wang, Y. Xian, L. Jin, Preparation of multiwall carbon nanotubes film modified electrode and its application to simultaneous determination of oxidizable amino acids in ion chromatography, Tanaka, Talanta 60 (2003) 1123–1130.
[27] L. Liu, F. Zhao, F. Xio, B. Zeng, Improved voltammetric response of L-tyrosine on multiwalled carbon nanotubes-ionic liquid composite coated glassy electrodes in the presence of cupric ion, Electroanalysis 20 (2008) 2148–2152.
[28] H. Liang, T. Ling, J.F. Rick, T. Chou, Molecularly imprinted electrochemical sensor able to enantroselectivly recognize d and L-tyrosine, Anal. Chim. Acta 542 (2005) 83–89.
[29] L. Wang, C. Ma, X. Zang, Y. Ren, Y. Yu, Determination of tyrosine traces by adsorption voltammetry of its copper (II) complex, Fresenius J. Anal. Chem. 351 (1995) 689–691.
[30] A. Babaei, S. Mirzakhani, B. Khalilzadeh, A sensitive simultaneous determination of epinephrine and tyrosine using an iron(III) doped zeolite-modified carbon paste electrode, J. Braz. Chem. Soc. 20 (2009) 1862–1869.
[31] G. Zhao, Y. Qi, Y. Tian, Simultaneous and direct determination of tryptophan and tyrosine at boron-doped diamond electrode, Electroanalysis 18 (2006) 830–834.
[32] Q. Xu, S. Wang, Electrocatalytic oxidation and direct determination of L-tyrosine by square wave voltammetry at multi-wall carbon nanotubes modified glassy carbon electrodes, Microchim. Acta 151 (2005) 47–52.
[33] Z. Chen, K. Okamura, M. Hanaki, T. Nagaoka, Differential pulse polarographic determination of uranium(VI) in complex materials after adsorption of its trifluoroethylxanthate cetyltrimethylammonium ion-associated complex on naphthalene adsorbent, Anal. Sci. 18 (2002) 427–432.
[34] V. Saumya, K.P. Prathish, T.P. Rao, In situ copper oxide modified molecularly imprinted polypyrrole film based voltammetric sensor for selective recognition of tyrosine, Talanta 85 (2011) 1056–1062.
[35] P. Kanchana, N. Lavanya, C. Sekar, Development of amperometric L-tyrosine sensor based on Fe-doped hydroxyapatite nanoparticles, Mater. Sci. Eng. C 35 (2014) 85–91.
[36] C. Quintana, S. Suarez, L. Hernandez, Nanostructures on gold electrodes for the development of an L-tyrosine electrochemical sensor based on host-guest supramolecular interactions, Sens. Actuators B Chem. 149 (2010) 129–135.
[37] Y. Liu, Z. Yang, Y. Zhong, J. Yu, Construction of europium hexacyanoferrate film and its electrocatalytic activity to tyrosine determination, Appl. Surf. Sci. 256 (2010) 3148–3154.
[38] X. Yu, Z. Mai, Y. Xiao, X. Zou, Electrochemical behavior and determination of L-tyrosine at single-walled carbon nanotubes modified glassy carbon electrode, Electroanalysis 20 (2008) 1246–1251.
[39] M. Taei, G. Ramazani, Simultaneous determination of norepinephrine, acetaminophen and tyrosine by differential pulse voltammetry using Au-nanoparticles/poly(2-amino-2-hydroxymethyl-propane-1,3-diol) film modified glassy carbon electrode, Colloids Surf. B 123 (2014) 23–32.
[40] U. Yogeswaran, S. Thiagarajan, S.M. Chen, Pinecone shape hydroxypropyl-β-cyclodextrin on a film of multi-walled carbon nanotubes coated with gold particles for the simultaneous determination of tyrosine, guanine, adenine and thymine, Carbon 45 (2007) 2783–2796.
[41] A.G. Gonzalez, M.A. Herrador, A.G. Asuero, Intra-laboratory testing of method accuracy from recovery assays, Talanta 48 (1999) 729–736.
[42] J.A. Arancibia, G.M. Escandar, Two different strategies for the fluorimetric determination of piroxicam in serum, Talanta 60 (2003) 1113–1121.